Solution Structure of Δ^5-3-Ketosteroid Isomerase Complexed with the Steroid 19-Nortestosterone Hemisuccinate[†,‡]

Michael A. Massiah,[§] Chitrananda Abeygunawardana,[§,||] Apostolos G. Gittis,[⊥] and Albert S. Mildvan*[,§]

Department of Biological Chemistry, The Johns Hopkins University School of Medicine, Baltimore, Maryland 21205, and Department of Biophysics, The Johns Hopkins University, Baltimore, Maryland 21218

Received June 18, 1998; Revised Manuscript Received August 13, 1998

ABSTRACT: The solution structure of the ketosteroid isomerase homodimer complexed with the product analogue 19-nortestosterone hemisuccinate (19-NTHS) was solved by heteronuclear multidimensional NMR methods using 1647 distance restraints, 77 dihedral angle (ϕ) restraints, and 67 hydrogen bond restraints per monomer. The refined secondary structure of each subunit consists of three α-helices, eight β-strands, four turns, and two β-bulges. The β-strands form a mixed β-sheet. One of the five proline residues, Pro-39, is cis and begins a nonclassical turn. A self-consistent ensemble of 15 tertiary/quaternary structures of the enzyme dimer−steroid complex, with no distance violations greater than 0.35 Å, was generated by simulated annealing and energy minimization with the program X-PLOR. The mean pairwise RMSD of the secondary structural elements was 0.63 Å for the average subunit and 1.25 Å for the dimer. Within each subunit, the three α-helices are packed onto the concave surface of the β-sheet with a groove between them into which the steroid binds at a site defined by 14 intermolecular distances. In the productive complex, Tyr-14, from α-helix 1, approaches both Asp-99 and the 3-keto group of 19-NTHS while, from β-strand 1, the carboxylate of Asp-38 approaches the β-face of the steroid near C4 and C6, between which it transfers a proton during catalysis. Thus the solution structure of the isomerase−steroid complex can accommodate the catalytic diad mechanism in which Asp-99 donates a hydrogen bond to Tyr-14 which in turn is hydrogen bonded to the 3-oxygen of the steroid. While direct hydrogen bonding of Asp-99 to the steroid oxygen is less likely, it cannot be excluded. All other interactions of the steroid with the enzyme are hydrophobic. The dimer interface, which is between the convex surfaces of the β-sheets, is defined by 28 intersubunit NOEs between hydrophobic residues in the ^{13}C-filtered NOESY−HSQC spectrum of a ^{13}C/^{12}C-heterolabeled dimer. Both hydrophobic and polar interactions occur at the dimer interface which contains no space that would permit additional steroid binding. Comparison of the complexed enzyme with the solution structure of the free enzyme [Wu et al. (1997) *Science 276*, 415−418] reveals that the three helices change position in the steroid complex, becoming more closely packed onto the concave surface of the β-sheet, thus bringing Tyr-14 closer to Asp-99 and the substrate. Comparison of the enzyme−steroid complex in solution with the free enzyme in the crystalline state reveals similar differences between the positions of the helices.

Δ^5-3-Ketosteroid isomerase (KSI)[1] from *Pseudomonas testosteroni* (EC 5.3.3.1) is a homodimeric enzyme with 125 amino acid residues per subunit which catalyzes the conversion of Δ^5- to Δ^4-3-ketosteroid via a dienolic intermediate (*1*−*4*). Three amino acid residues have been shown by mutagenesis to be important for enzymatic activity, Tyr-14 (*5*), Asp-38 (*5*), and Asp-99 (*6*). Thus, mutations of Asp-38 to Asn and Tyr-14 to Phe resulted in $10^{5.6}$- and $10^{4.6}$-fold lower k_{cat} values, respectively, than that of wild-type isomerase. These effects were additive in the double mutant which had completely lost all of its 10^{10}-fold catalytic power, yet retained the ability to bind steroids (*5*). Mutation of Asp-99 to Ala resulted in a $10^{3.7}$-fold decrease in k_{cat} (*6*).

In the first step of the isomerase reaction (Figure 1), Asp-38 functions as the catalytic base, removing the axial proton from the C4 position of the steroid, concerted with polarization of the 3-keto group by Tyr-14 and the protonated carboxyl group of Asp-99, to form the dienolic intermediate. In the next step, Asp-38 adds the same proton to the axial C6 position of the steroid, as reketonization of the intermediate completes the reaction.

While base catalysis by Asp-38 is generally agreed upon, two mechanisms of acid catalysis by Tyr-14 and Asp-99 have been proposed (Figure 1). In mechanism A, both Tyr-14 and Asp-99 directly donate normal hydrogen bonds to the 3-keto oxygen of the substrate and to the enolate oxygen of the intermediate. Mechanism A is supported by model

[†] These studies were supported by NIH Grant DK28616 (to A.S.M.).

[‡] A complete listing of the distance restraints derived from NOE data and chemical shifts have been deposited at the Brookhaven Protein Data Bank (Chemistry Department, Brookhaven National Laboratory, Upton, NY) (file name r1buqmr) together with the atomic coordinates of the family of 15 acceptable structures (file name 1buq).

* To whom correspondence should be addressed.

[§] Department of Biological Chemistry.

[||] Present address: Merck and Co., Inc., West Point, PA 19486.

[⊥] Department of Biophysics.

[1] Abbreviations: KSI, ketosteroid isomerase; 19-NTHS, 19-nortestosterone hemisuccinate; NMR, nuclear magnetic resonance; NOE, nuclear Overhauser effect; NOESY, NOE spectroscopy; TOCSY, total correlation spectroscopy; HSQC, heteronuclear single-quantum coherence; DMSO, dimethyl sulfoxide; TSP, sodium 3-(trimethylsilyl)-propionate-2,2,3,3-d_4; RMSD, root-mean-square deviation.

10.1021/bi981447b CCC: $15.00 © 1998 American Chemical Society
Published on Web 09/30/1998

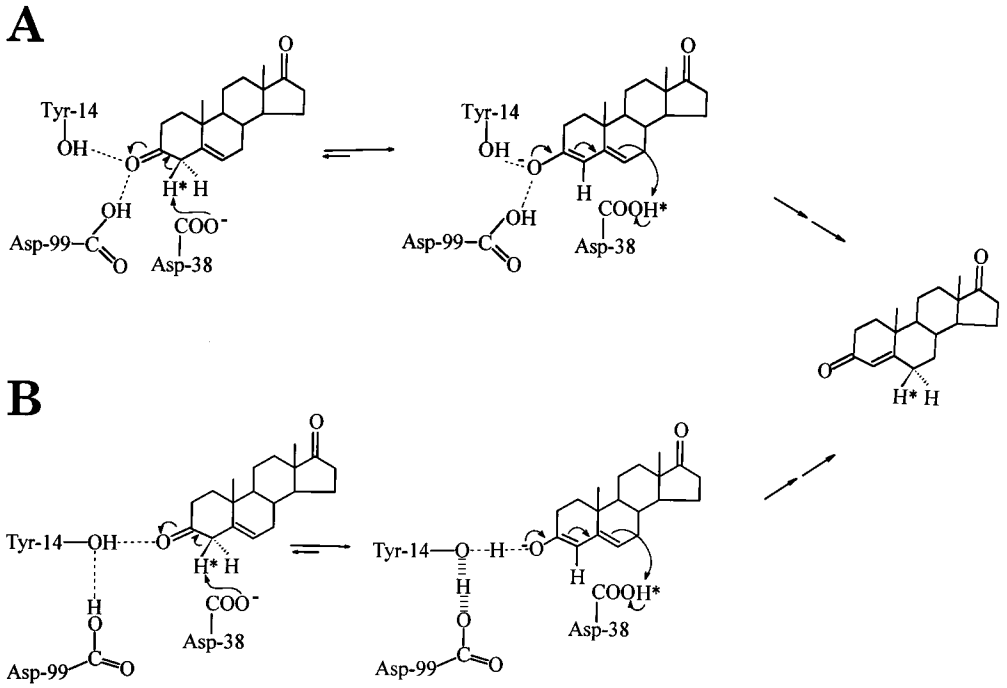

FIGURE 1: Alternative mechanisms of general acid catalysis in the Δ^5-3-ketosteroid isomerase reaction. (A) The intermediate is stabilized by two normal hydrogen bonds from Tyr-14 and Asp-99 (*6*). (B) The intermediate is stabilized by a catalytic diad involving a strong, low-barrier hydrogen bond from Asp-99 to Tyr-14 which strengthens the hydrogen bond from Tyr-14 to the intermediate (*8* and references therein).

building of the substrate into the NMR structure of the free enzyme (*6*), and by the 2.5 Å X-ray structure of the complex of a homologous isomerase from *Pseudomonas putida* with dihydroequilenin, an analogue of the intermediate (*7*).

Mechanism B involves a hydrogen-bonded catalytic diad Asp-99-COOH···Tyr-14-OH···O-steroid, consisting of normal hydrogen bonds in the substrate complex. As the intermediate dienolate forms, the hydrogen bond between Asp-99 and Tyr-14 increases in strength to form a low-barrier hydrogen bond. This strengthening effect is transmitted to the Tyr-14-OH···O-steroid in the transition state, facilitating polarization of the 3-keto group. Mechanism B is supported by NMR studies of highly deshielded protons at the active site of isomerase (*8*) and by mutagenesis studies which reveal the loss of both hydrogen bonds when Tyr-14 is mutated to Phe and the loss of the Asp-99 low-barrier hydrogen bond when Asp-99 is mutated to Ala (*6*, *8*).

To resolve this issue, further structural studies in solution are required. We have previously reported the solution secondary structure of isomerase complexed with 19-NTHS, a product analogue and substrate of the reverse isomerase reaction (*9*). In this paper, we describe the tertiary and quaternary solution structure of the isomerase homodimer complexed with 19-NTHS determined by heteronuclear multidimensional NMR spectroscopy. Preliminary abstracts of this work have been published (*10*, *11*).

Recently, the solution structure of free isomerase has been solved (*6*), permitting comparison of the free and steroid-complexed enzymes in solution. The X-ray structures of the free enzyme from *Ps. testosteroni*, at 2.3 Å resolution (*12*), and the homologous enzyme from *Ps. putida*, both free (at 1.9 Å resolution) and complexed with the intermediate analogue dihydroequilenin (at 2.5 Å resolution), have been reported (*7*), permitting comparison of the enzyme in the crystalline state and in solution.

EXPERIMENTAL PROCEDURES

Materials

The highly active Y55F/Y88F double mutant of isomerase, in which Tyr-14 is the only tyrosine residue, was used throughout this paper. The k_{cat}/K_m of this mutant is 80% that of the wild-type enzyme (*13*). Expression and purification of ^{13}C- and ^{15}N-labeled isomerase were carried out as previously described (*9*). The product analogue and substrate of the reverse isomerase reaction, 19-NTHS, was synthesized as previously reported (*13*). This steroid was used because of its solubility (*14*) and because it binds to the active site exclusively with its 3-keto group oriented inward, toward the side chain of Tyr-14 (*13*). The heterolabeled sample used for the $^1H-^{13}C$-filtered NOESY−HSQC spectrum was prepared by adding 250 μM (final concentration) each of $^{13}C/^{15}N$-labeled and ^{15}N-labeled KSI containing 10 mM sodium phosphate, 20 mM NaCl, 1.1 mM 19-NTHS (dissolved in DMSO-d_6), and 9% (v/v) DMSO-d_6 in D_2O at pH 7.2 and refrigerating for 4 weeks at 2 °C to permit the heterodimer to form and equilibrate.[2] The enzyme was shown to be fully active enzymatically and structurally identical after 1 year, based on assay and the observation that the $^1H-^{15}N$ correlations in the $^1H-^{15}N$ HSQC spectra did not show resonance shifts over this period (*9*).

Methods

NMR Spectroscopy. The 3D $^1H-^{13}C$-filtered NOESY−HSQC spectrum (*15*, *16*) was recorded at 37 °C on a Varian UnityPlus 600 MHz spectrometer equipped with a pulse field gradient unit, four independent RF channels, and a Varian 5 mm triple resonance probe with an actively shielded *z*-

[2] We thank R. M. Pollack for suggesting this procedure.

gradient. The data were recorded using the States−TPPI method (*17*) in all indirect dimensions, with a relaxation delay of 1.5 s.

The 3D ^{1}H−^{13}C-filtered NOESY−HSQC spectrum was collected with a 100 ms mixing time and spectral widths of 10 000 Hz (^{1}H, t_3, 1280 complex points), 960 Hz (^{1}H, t_2, 16 complex points) with the ^{1}H carrier frequency set at 1.3 ppm, and 2562 Hz (^{13}C, t_1, 16 complex points) with the ^{13}C carrier frequency set to 21.5 ppm. A total of 384 transients per hypercomplex t_1,t_2 pair was collected.

The 2D NOESY spectra (*18*, *19*) of a 600 μM unlabeled isomerase−19-NTHS complex in D_2O were collected as follows: 35, 50, and 100 ms mixing times, spectral widths of 8000 Hz (^{1}H, t_2, 4096 complex points) and 6600 Hz (^{1}H, t_1, 1024 complex points), and 32 transients per hypercomplex t_1,t_2 pair.

The ^{1}H−^{13}C-edited NOESY−HSQC spectrum was collected on a 600 μM ^{15}N/^{13}C uniformly labeled isomerase−19-NTHS sample as follows: 100 ms mixing time, spectral widths of 8400 Hz (^{1}H, t_3, 1024 complex points), 4525 Hz (^{13}C, t_2, 256 complex points) with the ^{13}C carrier frequency set to 43 ppm, and 7500 Hz (^{1}H, t_1, 1024 complex points), and 16 transients per hypercomplex t_1,t_2 pair (*9*).

The 3D ^{1}H−^{15}N HNHA spectrum (*20*) was collected with spectral widths of 8000 Hz (^{1}H, t_3, 1024 complex points), 6800 Hz (^{1}H, t_2, 64 complex points), and 1800 Hz (^{15}N, t_1, 64 complex points) using 64 transients per hypercomplex t_1,t_2 pair. The latter two experiments were collected using a Nalorac 8 mm triple resonance, pulse field gradient probe and with a 2.2 cm sample column (850 μL) in Shigemi 8 mm NMR tubes.

The ^{1}H−^{15}N NOESY−HSQC spectra were obtained and processed as previously described (*9*).

Data Processing. The NMR data were processed on an Indigo^{2}XZ Silicon Graphics workstation using the Felix 2.3 software package (Biosym Technologies). The t_3 (f_3) dimension of the 3D ^{1}H−^{13}C-filtered NOESY−HSQC was processed by applying an 80°-shifted sinebell square (ss) window function to the 680 points of the FIDs, followed by Fourier transformations and zero-order polynomial baseline corrections. The size of the processed spectrum was redefined to be 512 points so as to match the matrix size in the f_1 dimension. Exponential multiplication of the truncated t_2 (^{1}H) and t_1 (^{13}C) of known phase was followed by linear prediction with mirror image constraints to yield a real data set three times it original size (*21*). Apodization with a 90°-shifted sinebell window function was applied, followed by zero-filling in both the t_2 and t_1 dimensions to 128 points to yield a final matrix size of 128 (f_1) × 128 (f_2) × 512 (f_3) real data points. For the 3D ^{1}H−^{13}C-filtered NOESY−HSQC spectrum, t_3 and t_1 dimensions were processed by applying 80°-shifted sinebell square (ss) window functions to the FIDs and interferogram, respectively, followed by Fourier transformations and zero-order polynomial baseline corrections. Apodization with a 90°-shifted sinebell window function was applied, followed by zero-filling in the t_2 dimensions to 256 points to yield a final matrix size of 256 (f_1) × 512 (f_2) × 1024 (f_3) real data points. The HNHA spectrum was processed similarly to the aforementioned spectrum, except that the data size in the t_3 dimension (^{1}H) was redefined to be 256 points to include only the NH region of the spectrum and to yield a matrix size of 128 (f_1) × 128 (f_2) × 256 (f_3) real data points. The 2D NOESY spectra were processed by applying 80°-shifted sinebell square (ss) window functions to both t_1 and t_2, followed by zero-filling in t_1, Fourier transformations, and zero-order polynomial baseline corrections to yield a 2048 × 1024 point real data matrix. The observed ^{1}H chemical shift was referenced with respect to the H_2O or HDO signal, which was taken as 4.658 ppm downfield from external TSP at 37 °C, and the ^{13}C chemical shifts are given with respect to external TSP in D_2O (0.00 ppm). All data analysis was done using the NMRVIEW 2.1 software package (*22*).

Structural Calculations. Distance restraints of 1.8−2.8, 1.8−3.2, and 1.8−5.0 Å were employed for NOE cross-peaks of strong, medium, and weak intensity, respectively, observed in the 2D and 3D ^{15}N- and ^{13}C-edited NOESY spectra obtained with 100 ms mixing times. An additional 1.0 Å was added for NOEs involving methyl protons, and a correction of 2.3 Å was added to restraints for NOEs involving degenerate Hδ or Hϵ protons of tyrosine and phenylalanine. Hence, the distances between Tyr-14 Hϵ protons and the equatorial and axial protons at the C2 position of 19-NTHS, which were previously measured to be 3.1 and 4.2 Å (*13*), were assigned upper limit values of 5.4 and 6.5 Å, respectively. Two previously reported interproton distances, estimated from interproton NOEs involving highly deshielded proton resonances of Asp-99-COOH (at 18.2 ppm) and Tyr-14-OH (at 11.6 ppm), were used from the complex of the D38N mutant of isomerase with dihydroequilenin, an analogue of the intermediate (*9*). Such deshielded proton resonances are detectable only in complexes of isomerase with analogues of the intermediate (*4*, *8*). These interproton distances were from Tyr-14 Hϵ to Asp-99-COOH (2.8−5.1 Å) and from Tyr-14-OH to Asp-99-COOH (2.6 ± 0.2 Å). In addition, the O−H···O hydrogen bond distance from Tyr-14 to the steroid oxygen was set to 2.7 ± 0.04 Å from its proton chemical shift of 11.6 ppm together with a correlation of proton chemical shifts with hydrogen bond distances in the solid state (*8*, *23*) and from its fractionation factor of 0.97 (*8*, *24*, *25*). By the same methods, the hydrogen bond distance from Asp-99-COOH to Tyr-14-OH, based on the chemical shift of 18.2 ppm and fractionation factor of 0.34, was set at 2.45 ± 0.15 Å.

For the H$\alpha_{(i)}$−H$\alpha_{(i+1)}$ distance between Asp-38 and Pro-39, a lower limit of 2.2 Å was assigned to maintain a *cis*-peptide bond as observed (see Results and Discussion). Hydrogen bond restraints were applied as square-well distance potentials between the hydrogen bond-accepting carbonyl oxygens of the protein and both the hydrogen bond-donating NH groups and N atoms with ranges between 1.5−2.5 and 2.5−3.5 Å, respectively. While the ^{13}C-filtered spectra identified intersubunit NOEs, values for the distance restraints between the residues at the subunit interface were determined on the basis of NOE intensities in the ^{13}C-edited NOESY. Dihedral angle, ϕ, restraints were determined from $^3J_{NH\alpha}$ values calculated from the 3D HNHA spectrum (*20*). Dihedral angles of −60° ± 30° obtained from $^3J_{NH\alpha}$ values of 3.0−5.5 Hz and −120° ± 30° from $^3J_{NH\alpha}$ values of 7.0−9.0 Hz were used for residues in the α-helices and β-strands, respectively. Fourteen intramolecular distance restraints between the heavy atoms and protons of 19-NTHS based on its X-ray coordinates were implemented to keep the steroid conformation unchanged from that determined by

small molecule X-ray crystallography of 19-nortestosterone (*26*).

Distance geometry, simulated annealing, and refinement calculations were performed with X-PLOR 3.8 (*27*) operating on a 8-processor Silicon Graphics R10 000 Power Challenge computer. All atoms of the 250-residue homodimer and the two 19-NTHS ligands were included in the structure calculations. A set of 120 embedded substructures, based on 1647 distance restraints and 77 dihedral angle restraints per monomer, was generated using distance geometry and regularized by energy minimization against a distance geometry energy term (the sub-embed protocol in X-PLOR). After template fitting, the embedded substructures were further regularized by simulated annealing with a starting temperature of 2000 K and using 6000 steps in both the annealing and cooling stages with a time step of 1 fs. The resulting structures underwent a simulated annealing refinement of the slow-cooling type with a starting temperature of 2000 K and 6000 steps during the cooling stage with a time step of 1 fs, followed by 500 steps of energy minimization. During the refinement, the nonbonded interactions were modeled only by a quadratic repulsive energy term, while the attractive component of the Lennard-Jones potential and the electrostatic energy were turned off. At the final stages of refinement, a square-well potential energy function was used for the NOE and the dihedral angle restraints with a force constant of 50 kcal mol^{-1} $Å^{-2}$ and 200 kcal mol^{-1} rad^{-2}, respectively. Of the 120 embedded substructures, 60 converged to acceptable structures with NOE violations ≤ 0.5 Å. Of these, the 15 best structures with NOE violations ≤ 0.35 Å and dihedral violations $\leq 5°$ were selected.

Superpositioning of computed structures and calculations of RMSD values were performed with the MidasPlus software package.

RESULTS AND DISCUSSION

Side-Chain Stereospecific Assignments. Backbone and side-chain proton resonances in the isomerase−19-NTHS complex were previously assigned from triple resonance, 3D $^1H-^{15}N$ NOESY−HSQC, and 3D HCCH−TOCSY experiments (*9*). In the present work, the stereospecific assignments (i.e., *pro-R* and *pro-S*) for the side-chain methyl and methylene protons of the complex are established for 71 of the 154 prochiral centers in each protein subunit. Almost all of the methyl resonances of valine, leucine, and isoleucine residues (46 of 50) were stereospecifically assigned on the basis of intra- and interresidue NOE cross-peak patterns in the 3D $^1H-^{15}N$ NOESY−HSQC and 3D $^1H-^{13}C$ NOESY−HSQC spectra. Likewise, the stereochemistry of 96 of the 180 nondegenerate geminal β- and γ-protons were identified. These stereospecific assignments permit unambiguous identification of the long-range NOEs, resulting in more precise structure calculations. Aromatic side-chain proton resonances were assigned from the cross-peak patterns in the 2D NOESY in D_2O (100 ms) and from the coupling patterns in the previously reported 2D TOCSY (*9*). The complete stereochemical and sequence-specific ^1H, ^{15}N, and ^{13}C assignments for the KSI−NTHS complex are given as Supporting Information (Table S1).

Isomerase contains five proline residues, four of which were found to be in the *trans* conformation (Pro-4, Pro-44, Pro-62, Pro-97) and one in the *cis* conformation (Pro-39). The conformations of each of these proline residues are based on four criteria (*28*). For the *trans*-prolines, the NOE cross-peaks of $H^{\delta}_{(i)}-H^{\alpha}_{(i-1)}$ and $H^{\delta}_{(i)}-NH_{(i-1)}$ were present, and no $H^{\alpha}_{(i)}-H^{\alpha}_{(i-1)}$ or $H^{\alpha}_{(i)}-NH_{(i-1)}$ NOEs were observed. For the *cis*-proline, the $H^{\alpha}_{(i)}-H^{\alpha}_{(i-1)}$ and $H^{\alpha}_{(i)}-NH_{(i-1)}$ NOE cross-peaks were present and no $H^{\delta}_{(i)}-H^{\alpha}_{(i-1)}$ or $H^{\delta}_{(i)}-NH_{(i-1)}$ NOEs were observed.

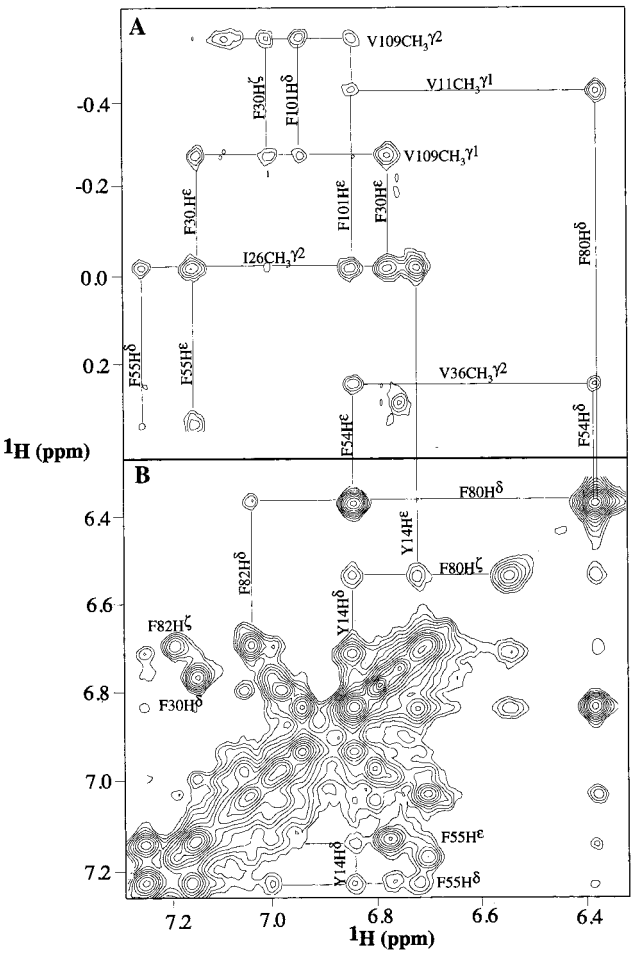

FIGURE 2: Regions of the 2D NOESY spectrum of the KSI−19-NTHS complex in D_2O showing NOE cross-peaks between the aromatic and methyl protons (A) and aromatic to aromatic protons (B). Many of these NOEs identify residues that either line the active site or form the hydrophobic core of the subunit.

Refined Secondary Structure. The detection and assignment of additional NOEs resulted in several refinements of the previously reported secondary structure (*9*). Helix 2 (residues 23−30), previously described as a 3_{10} helix, is now found to be an α-helix on the basis of the observation of three $\alpha_{(i)}-NH_{(i+4)}$ NOEs from residues Leu-23 to Val-27, Asp-24 to Ala-28, and Ile-26 to Tyr-30. The sequence, Ile-121 to Gly-124, previously described as unstructured, is now found to be a β-strand, based on three strong $\alpha_{(i)}-NH_{(i+1)}$ NOEs. This strand (β-strand 8) is aligned antiparallel with residues Ala-96 to Lys-92 of β-strand 6 on the basis of 20 cross-strand NOEs. Two β-bulges, defined by strong $NH_{(i)}-NH_{(i+1)}$ NOEs, are detected between β-strands 3 and 4 (residues 68−70) and between β-strands 7 and 8 (residues 117−120). The latter was previously described as a turn, but no change in direction occurs. The refined secondary structure now consists of three α-helices (residues 5−21,

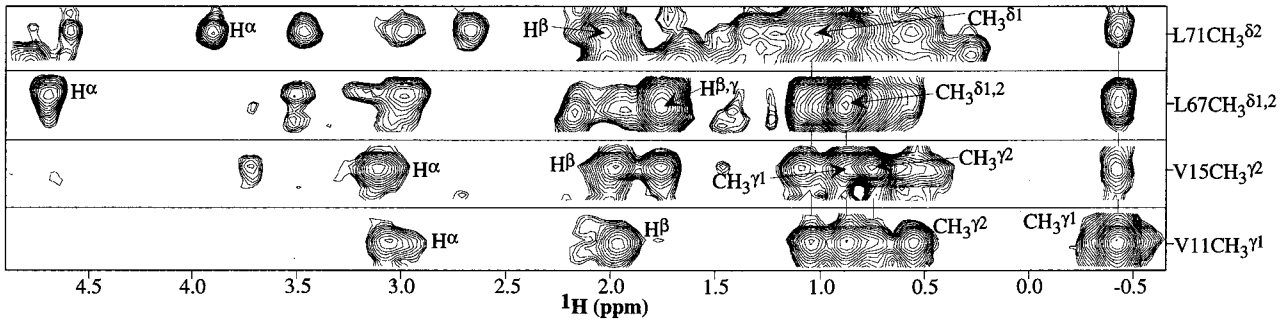

FIGURE 3: Upfield regions of the ^{13}C planes taken from the 3D $^{1}H-^{13}C$ NOESY−HSQC spectrum of the $^{15}N/^{13}C$-labeled KSI−19-NTHS complex. The lowest strip shows the ^{13}C plane for Val-11 $CH_3^{\gamma 1}$ (diagonal = −0.42 ppm) showing cross-correlations to Val-15 $CH_3^{\gamma 2}$ and the δ methyls of Leu-67 and Leu-71 side chains. These data provide information on the proximity and orientation of helix 1 with respect to the mixed β-sheet.

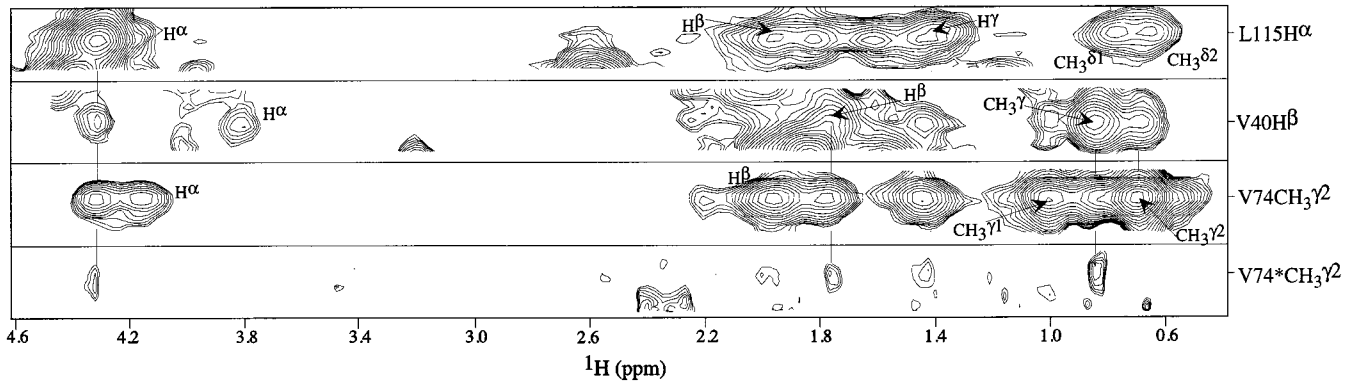

FIGURE 4: 3D $^{1}H-^{13}C$ NOESY−HSQC spectrum (upper three strips) and the 3D ^{13}C-filtered $^{1}H-^{13}C$ NOESY−HSQC spectrum obtained on a $^{13}C/^{12}C$ heterolabeled dimer (bottom strip, Val-74* $CH_3^{\gamma 2}$). Upfield regions of the ^{13}C planes through side-chain proton signals at the subunit interface are shown. The bottom strip exemplifies intersubunit NOEs between Val-74* $CH_3^{\gamma 2}$ from one subunit to Val-40 Hβ and Leu-115 Hα of the other subunit.

23−30, 48−60), eight β-strands (residues 34−38, 44−47, 63−67, 71−73, 78−87, 92−104, 111−116, 121−124) which form a mixed β-sheet, four turns (residues 39−43, 74−77, 88−91, 105−108), and two β-bulges (residues 68−70, 117−120). Thus, isomerase consists of 30% α-helix, 40% β-sheet, 13% turns, 6% β-bulges, and the remaining 14 residues (11%) are in coils.

NOEs Involving Side-Chain Protons and Hydrophobic Interactions. Making use of the assigned proton resonances, including the stereospecific assignments, and the refined secondary structure, tertiary structural information was obtained from the 2D NOESY (Figure 2) and the 3D $^{1}H-^{13}C$ NOESY−HSQC spectra (Figure 3). The quality of the data in the ^{13}C-edited NOESY permitted the unambiguous assignment of 338 long-range NOEs involving the side-chain protons of each subunit. In addition, nondegenerate β- and γ-methylene protons of amino acids that have side chains with more than one methylene group (Pro, Met, Glu, Gln, Lys, and Arg) were distinguished on the basis of their occurrence within single ^{13}C planes in the 3D ^{13}C-edited NOESY spectrum.

Two regions of the 2D NOESY spectrum showing well-resolved long-range NOEs from methyl to aromatic side-chain protons and from aromatic to aromatic side-chain protons are shown in panels A and B of Figure 2, respectively. Figure 2A shows the dipolar correlations indicating proximity between the Val-109 γCH_3 protons and the aromatic ϵ-protons of Phe-30 and Phe-101. Similarly, the Ile-26 $\gamma 2$-CH_3 protons show strong dipolar correlations to the ϵ-protons of Phe-101 and Phe-55 and to both the δ- and ϵ-protons of Phe-30. In addition, the data show the Val-11 γ-CH_3 (*pro-S*) to be in close proximity to the side chains of Phe-80 and Phe-101. Figure 2B shows NOEs between aromatic residues which indicate that the Phe-80 and Tyr-14 side chains are in close spatial proximity. All of these NOEs identify hydrophobic interactions of residues of the α-helices with each other as well as with residues of the β-sheet. Figure 2B also shows that, with the exceptions of Phe-88 and Phe-116, which are in the active site cleft and solvent exposed, all of the other Phe residues (Phe-30, 54, 55, 80, 82, and 86) are packed in a highly hydrophobic core together with the side-chains of Leu-18, -23, -29, -59, -61, -63, -67, and -71, Ile-26, and Val-10, -11, -15, -27, -36, and -71. This hydrophobic core helps to define the tertiary structure of each subunit. With the exception of His-100, no aromatic residues were found at the subunit interface of isomerase (see below).

Figure 3 shows $^{1}H-^{1}H$ ^{13}C strips from the upfield region of the 3D $^{1}H-^{13}C$ NOESY−HSQC spectrum identifying NOEs between the γ-CH_3 (*pro-R*) group of Val-11 to the γ-CH_3 (*pro-R*) group of Val-15 and to the δ-CH_3 (*pro-R*) groups of Leu-67 and Leu-71. These NOEs further indicate interactions between hydrophobic residues that form the core of the monomer and identify residues of helix 1 which pack onto the mixed β-sheet.

Subunit−Subunit Interactions. The dimer interface of isomerase was identified from NOE correlations in both the 3D $^{1}H-^{13}C$-filtered NOESY−HSQC of a $^{12}C/^{13}C$-hetero-labeled dimer and the 3D $^{1}H-^{13}C$ NOESY−HSQC spectra of a $^{15}N/^{13}C$ uniformly labeled protein (Figure 4). The upper

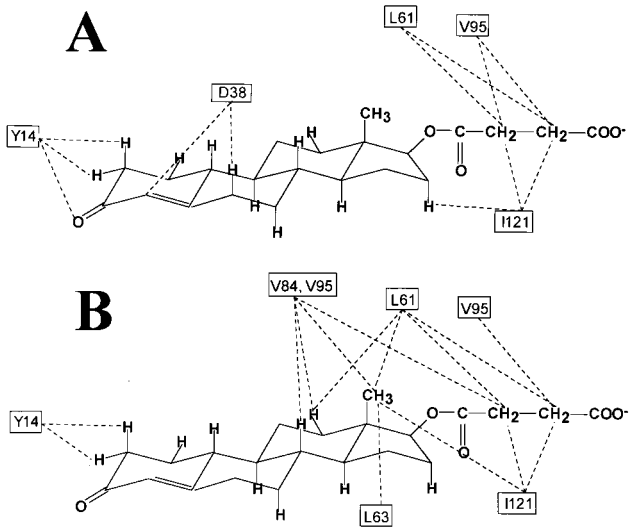

FIGURE 5: Intermolecular restraints used to position 19-NTHS into the active site of KSI. (A) The catalytically productive complex. The proximities of steroid protons to Tyr-14, Leu-62, Val-95, and Ile-121 are based on NOEs (*9*, *13*). The hydrogen bond from Tyr-14 OH to the 3-keto oxygen is based on its proton chemical shift and fractionation factor (*8*). The proximities of Asp-38 to the C4 and C6 positions of the steroid are based on the tunneling contribution to the proton transfer between the steroid and Asp-38 (*31*). (B) The nonproductive mode of steroid binding. The proximities are all based on NOEs (*9*).

three ^{13}C strips of Figure 4 show both intra- and intersubunit NOE cross-peaks between Leu-115, Val-40, and Leu-74 side-chain protons in the 3D $^{1}H-^{13}C$ NOESY−HSQC spectrum. Analysis of these NOEs would place the Val-40 side chain from one edge of the β-sheet near the Val-74 side chain at the opposite edge of the β-sheet. This interaction was found to be intersubunit, as indicated by the bottom strip of Figure 4, taken from the $^{1}H-^{13}C$-filtered spectrum of the heterolabeled dimer, which reveals intersubunit NOEs from Leu-74 γ-$^{13}CH_3$ (*pro-R*) to side-chain protons of Val-40′ and Leu-115′. If these interactions had been intrasubunit, gross distortion of the monomers would have resulted. By this method, 28 intersubunit NOEs were identified between the hydrophobic residues at the dimer interface. These intersubunit NOEs were from Val-74 to Leu-115′, Val-74 to Gly-117′, Val-74 to Val-40′, Ala-79 to Leu-115′, Ala-79 to Ile-98′, Ala-75 to Val-40′, and Ala-75 to Gly-41′. Due to the limited sensitivity of the data obtained from the 250 μM heterolabeled dimer sample, no intersubunit NOEs were observed between side-chain protons of polar residues that are also present in the dimer interface (see below).

Enzyme−Steroid Interactions. The interaction of steroids with isomerase has long been known to be complicated by nonproductive binding at the active site (*29*, *30*). Most of the NOEs detected between 19-NTHS and the enzyme indicate strong hydrophobic interactions exemplified by 11 NOEs from the axial 18-CH_3 group of the steroid to the side-chain protons of Val 84, Val-95, Ile-121, Leu-61, and Leu-63 (*9*). Although effective in locating the active site, these interactions represent a nonproductive enzyme−substrate complex since it would place C4 and C6 of the steroid far from the general base, Asp-38, which transfers a proton between them during catalysis. Attempts to simultaneously fit all of the intermolecular transferred NOEs between the enzyme and 19-NTHS resulted in structures with numerous distance violations, high van der Waals penalties, and multiple orientations and distortions of the bound steroid, indicating some of these NOEs to be mutually inconsistent. While multiple modes of steroid binding to isomerase are well established (*29*, *30*), the possibility that some of these NOEs may have resulted from spin diffusion within the hydrophobic binding pocket cannot be excluded.

Table 1: NMR Restraints and Structural Statistics for the Productive Isomerase−19-NTHS Complex

X-PLOR Input Restraints	
intramolecular NOEs for KSI	
sequential ($\|i-j\|=1$)	431
medium range ($1<\|i-j\|\le 5$)	200
long range ($\|i-j\|>5$)	338
intraresidue	650
intersubunit	28
total NOEs	1647
NOEs/residue	13.2
hydrogen bonds	67
dihedral angles (ϕ)	77
intramolecular restraints for NTHS	5
intermolecular NOEs between KSI and NTHS	14

Average RMSD from Idealized Geometry of 15 Structures	
bonds (Å)	$4.59\times10^{-3}\pm3.01\times10^{-5}$
angles (deg)	$7.39\times10^{-1}\pm5.81\times10^{-3}$
impropers (deg)	$7.93\times10^{0}\pm3.39\times10^{-3}$

Pairwise RMSD of an Ensemble of 15 Calculated Structures (Å)	subunit 1	subunit 2	dimer
backbone of secondary structure[a]	0.61 ± 0.09	0.65 ± 0.14	1.25 ± 0.42
all atoms, secondary structure	1.65 ± 0.12	1.66 ± 0.18	2.00 ± 0.28
all atoms, secondary KSI−NTHS	1.65 ± 0.12	1.65 ± 0.19	1.99 ± 0.28
backbone of residues 1−125	1.02 ± 0.16	1.02 ± 0.14	1.58 ± 0.41
all atoms, residues 1−125	1.96 ± 0.16	1.96 ± 0.17	2.33 ± 0.31
all atoms, KSI−NTHS	1.96 ± 0.15	1.95 ± 0.17	2.31 ± 0.30
all atoms, NTHS	0.99 ± 0.14	0.96 ± 0.14	1.44 ± 0.34

[a] Residues superimposed of the secondary structural elements for the KSI−NTHS complex are 5−21, 23−30, 34−38, 44−47, 48−60, 63−67, 71−73, 78−87, 92−104, 111−116, and 121−124.

Figure 5A summarizes the limited number of measured intermolecular restraints used to position the substrate in a productive complex consistent with the catalytic activity and stereoselectivity of the enzyme. These restraints consist of NOEs from the protons of the succinyl moiety and the D-ring of 19-NTHS to hydrophobic residues of isomerase (*9*) and from the axial and equatorial C2 protons of 19-NTHS to Tyr-14 CϵH (*13*). Other restraints are based on the established hydrogen bonding between Tyr-14 and the 3-oxygen of the steroid 19-NTHS (*13*), estradiol, and dihydroequilenin (*8*). In addition, NOEs from Asp-99 Hβ1 and Hβ2 to Tyr-14 Hϵ in the 19-NTHS complex and from Asp-99-COOH to Tyr-14-OH and to Tyr-14 Hϵ in the estradiol and dihydroequilenin complexes (*8*) were used to help to define the hydrogen-bonding network. Finally, the carboxylate oxygens of Asp-38 were restrained to be 3.0 ± 0.5 and 2.2 ± 0.3 Å from C4 and the axial C6H of 19-NTHS, respectively, consistent with the enzyme-catalyzed stereoselective proton transfer between these two positions of the substrate and with the proton tunneling detected between the steroid substrate and Asp-38 (*31*).

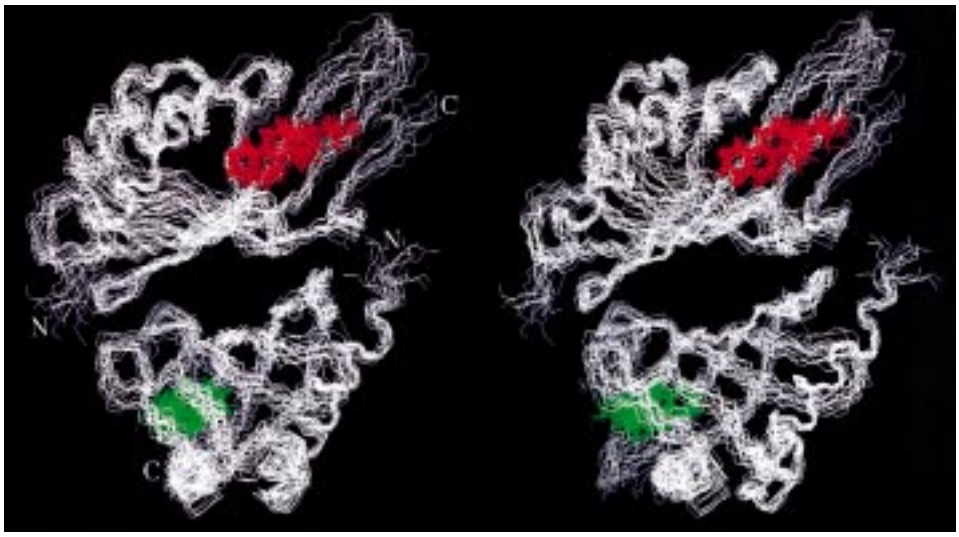

FIGURE 6: Stereopair of the superposition of 15 acceptable computed structures of the Δ^5-3-ketosteroid isomerase dimer complexed with 19-NTHS in the catalytically productive orientation. The bound steroids are shown in red in the upper subunit and in green in the lower subunit.

The remaining 11 NOEs between 19-NTHS and the enzyme (Figure 5B) which were incompatible with productive steroid binding were used to define a single, nonproductive orientation of the bound steroid (see below). Additional nonproductive steroid binding modes, such as backward binding, apparently are suppressed by the charged hemisuccinate group at position 17.

Tertiary Structure Calculation and Refinement. To eliminate NOEs that might be due to spin diffusion, a simple protocol was followed: protons that exhibit NOEs to a specific prochiral proton often give rise to a weaker intensity NOE cross-peak to the neighboring prochiral proton. Likewise, the prochiral methyl groups of leucine and valine residues show the same pattern. Since spin diffusion is likely to contribute to the weaker signal, and since restraints derived for the weaker of two such NOEs are redundant in the structure calculation, distance restraints were not employed for these weak NOE cross-peaks. Using this protocol, ~25% of the NOE cross-peaks observed in the NOESY spectra were not used in the structure calculations. As a result of this protocol, a total of 1647 distance restraints (13.2 per residue) were used for each subunit from the NOE data including 338 long-range, 200 medium-range, 431 sequential, and 650 intraresidue NOEs (Table 1). A total of 77 $^3J_{NH\alpha}$ values were determined in the 3D HNHA spectrum and used as backbone dihedral angle, ϕ, restraints for each KSI subunit. Values of $^3J_{NH\alpha}$ ranging from 3.0 to 5.5 Hz were used to determine the ϕ dihedral angle restraints for the α-helices, and values from 7.0 to 9.0 Hz were used for the β-strands. On the basis of the refined secondary structure, 65 backbone hydrogen bonds, 30 for the α-helices and 35 for the mixed β-sheet, and 2 side-chain hydrogen bonds, were used as additional restraints for each subunit in the structure calculation.

Description of the Tertiary Structure. Figure 6 shows the backbone C_α, C′, and N atom superposition of the secondary structural elements of 15 dimeric structures of the isomerase−19-NTHS complex that have no NOE violations exceeding 0.35 Å and no dihedral angle violations exceeding 5° (Table 1). All of the dimeric structures, i.e., a total of 250 residues each, and the locations of the two bound 19-NTHS substrates were generated ab initio from random conformations.

FIGURE 7: Structure of the lowest energy conformation of the Δ^5-3-ketosteroid isomerase dimer complexed with 19-NTHS. The protein is in green, the steroid is in red, and catalytic residues Tyr-14, Asp-38, and Asp-99 are in yellow. The figure was generated and rendered with the Molscript (*34*) and Raster3D (*35*) software packages, respectively.

Coordinates for the conformation of 19-NTHS were taken from the high-resolution small molecule X-ray structure of 19-nortestosterone (*26*) to which was appended protons and the succinyl moiety at the C17-OH position. As indicated from the backbone superposition, the tertiary and quaternary structures of the enzyme are reasonably well defined with a pairwise RMSD value of 1.25 Å when the backbone secondary structural elements are superimposed (Table 1). Due to the lack of long-range NOEs, the positions of

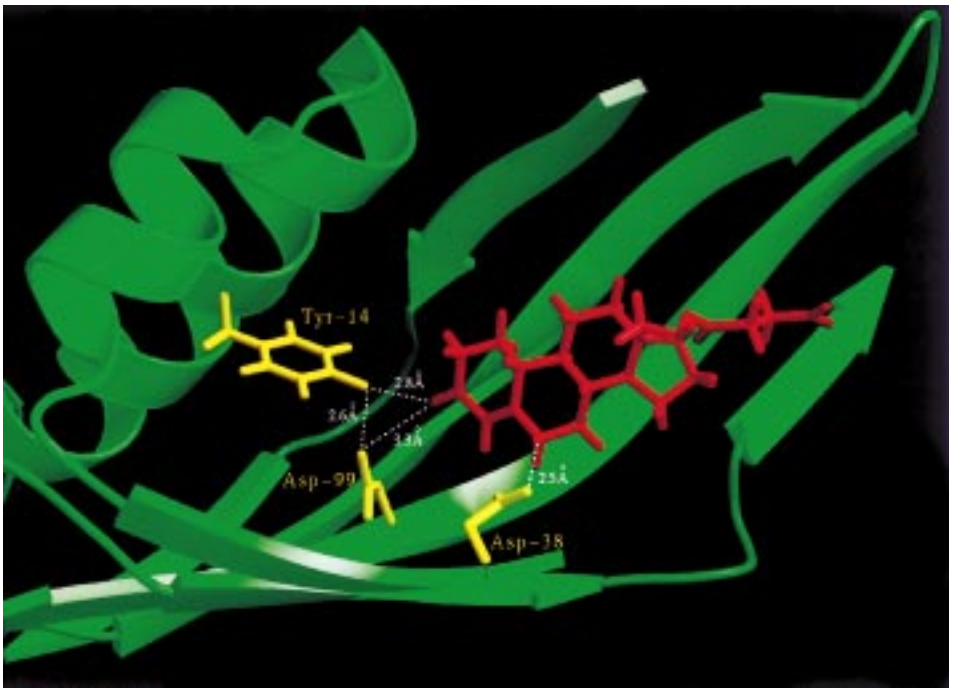

FIGURE 8: Active site of isomerase showing distances from catalytic residues to 19-NTHS averaged over the 15 acceptable structures. The steroid is bound in a catalytically productive orientation.

backbone atoms of residues between β-strands 5 and 6 (Asn-104 to Ser-108), β-bulge 1 (Thr-68 to Glu-70), and β-bulge 2 (Gly-117 to Asn-120) are not precisely defined. Similarly, the exposed segment of the β-sheet consisting of residues 86−94 on strands 5 and 6 and residues 121−125 on strand 8 shows diffuse positions of the backbone atoms. Pairwise superposition of all atoms between residues Met-1 and Ala-125 yields an RMSD value of 2.33 ± 0.31 Å. The Ramachandran diagrams of all of the calculated structures reveals 70 ± 2% of the residues to be in the most favored regions, 25 ± 2% of the residues to be in the favored regions, and less than 1% of the residues to be outside the allowed range of $\phi\psi$ values.

Figure 7 shows the structure with the lowest van der Waals and NOE energies. The three-dimensional structure of the protein consists of two identical subunits, each containing three α-helices and eight β-strands. The β-strands form a mixed β-sheet (*9*) which is curved, with concave and convex surfaces. The helices are stacked onto the concave surface of the β-sheet. The tertiary structure of the monomer reveals extensive hydrophobic packing that includes all but two aromatic side chains (Phe-88, Phe-116). Helix 1 (Glu-5 to Gly-21) contains the catalytic Tyr-14 residue and lies in close proximity to Asp-99 on β-strand 6. Asp-99 is surrounded by the hydrophobic side chains of residues Phe-80, Phe-82, Phe-55, Phe-30, Leu-18, and Val-15. Helix 2 (Leu-23 to Phe-30) lies almost antiparallel to helix 1, at an angle of ~150° and makes extensive hydrophobic contacts with helices 1 and 3 as well as with the β-sheet. Helix 3, consisting of residues Thr-48 to Lys-60, connects β-strands 2 (Ser-44 to Gly-47) and 3 (Leu-63 to Leu-67) which constitute the extreme edges of the β-sheet. This remote connection by helix 3 results in a concavity in the β-sheet which faces all of the helices, creating a groove into which the steroid substrate binds (Figures 7 and 8). This steroid binding site is lined by hydrophobic residues. The length of helix 3 may be critical since amino acid deletion or insertion in this helix could change the curvature of the β-sheet, which in turn could affect the proximity of the Asp-99 and Tyr-14 side chains.

Active Site and Mechanistic Considerations. Each steroid binds in a groove between the three α-helices and the concave surface of the mixed β-sheet, interacting only with residues of one subunit. The environment of the bound steroid is highly hydrophobic, consisting of residues Val-15, Leu-18, Leu-29, Val-36, Phe-54, Phe-55, Leu-61, Leu-63, Phe-80, Phe-82, Val-85, Phe-86, Val-95, Phe-116, and Ile-121. Exceptions are the catalytic residues, Asp-38, Tyr-14, and Asp-99, as well as Ser-58 which approaches C10 and C11 of the steroid but is too far from Tyr-14-Oζ, Asp-38-Oδ, and Asp-99-Oδ (~8 Å) to participate in catalysis. Figure 8 shows the active site occupied by 19-NTHS in the lowest energy structure of isomerase. The distance between the side-chain oxygen atoms of Asp-99 and Tyr-14 is 2.61 ± 0.03 Å averaged over the 15 structures, consistent with a strong hydrogen bond. The distance from the oxygen atom of Tyr-14 to the 3-keto oxygen of the steroid of 2.80 ± 0.06 Å indicates a normal hydrogen bond, while the distance from the nearest carboxyl oxygen of Asp-99 to the 3-keto oxygen of the steroid of 3.25 ± 0.39 Å indicates at best, a weak hydrogen bond. These results are consistent with the catalytic diad mechanism (Figure 1B) (*8*) but do not exclude a direct interaction of Asp-99 with the steroid as in Figure 1A. The catalytic diad is consistent with the observations that the Y14F mutation abolishes the deshielded resonances at 18.2 and 11.6 ppm of both Asp-99-COOH and Tyr-14-OH, respectively (*4*, *8*) while the D99A mutation abolishes only the deshielded proton resonance of Asp-99-COOH (*6*). It is also consistent with the complete loss of catalytic activity in the Y14F + D38N double mutant (*5*).

Asp-38 approaches the β-face of the steroid with its carboxylate oxygens at distances of 3.50 ± 0.08 Å from C4 and 2.96 ± 0.33 Å from C6, in accord with its catalytic role in transferring protons between these two positions (Figure

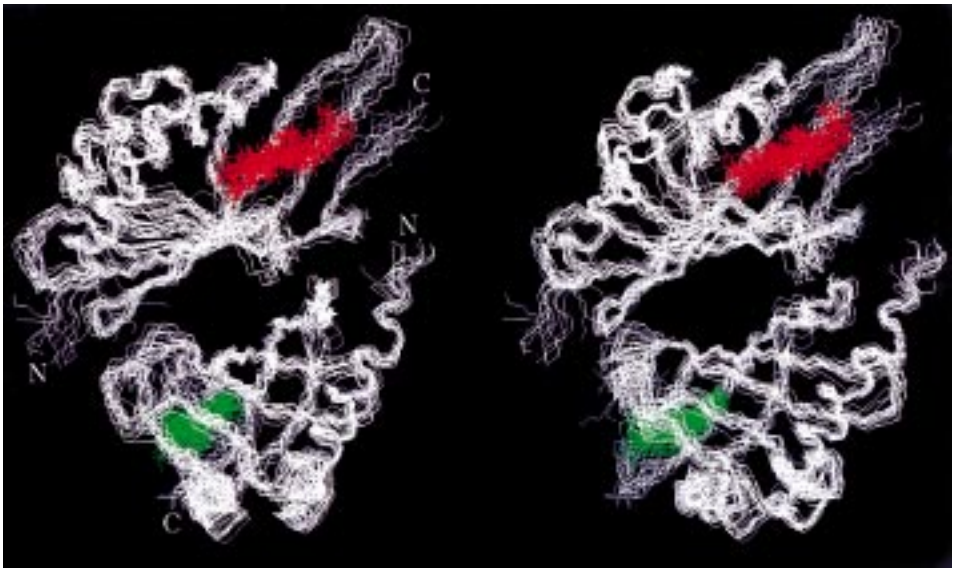

FIGURE 9: Stereopair of the alternative mode of 19-NTHS binding to isomerase in a nonproductive orientation as discussed in the text. Fifteen acceptable structures are superimposed.

1). The carboxylate group of Asp-38 is too far from Tyr-14 (6.34 ± 0.58 Å) and from Asp-99 (7.56 ± 0.79 Å) to participate in the hydrogen bond network, in accord with the observation that mutation of Asp-38 to Asn did not alter the deshielded proton resonances of Asp-99-COOH (at 18.2 ppm) or of Tyr-14-OH (at 11.6 ppm) (*4*, *8*) and with the simple additive effects on catalysis of the Y14F and D38N mutations (*5*).

Control computations of 60 structures, omitting the short, strong hydrogen bond between Asp-99-COOH and Tyr-14-OH of 2.45 ± 0.15 Å based on the proton chemical shift and fractionation factor, yielded 28 acceptable structures with no NOE or dihedral violations ≥0.35 Å and 5°, respectively. The distance between the side-chain oxygen atoms of Asp-99 and Tyr-14 increases and shows much greater variability, 3.98 ± 0.55 Å (range 2.74−4.70 Å). The side-chain oxygen of Asp-99, however, remains far from the steroid oxygen, 3.82 ± 0.66 Å (range 2.83−5.24 Å), indicating in both cases weak or no hydrogen bonding. The restrained distance from Tyr-14-Oζ to the steroid oxygen remains at 2.78 ± 0.08 Å.

Despite the absence of NOEs between Asp-99 and the steroid, separate control computations were made placing a strong hydrogen bond between Asp-99-COOH and the steroid oxygen, retaining the hydrogen bond from Tyr-14-OH to the steroid oxygen, and omitting the hydrogen bond from Asp-99-COOH to Tyr-14-OH, as in the mechanism of Figure 1A. In 28 acceptable structures, the distance from the side-chain oxygen of Asp-99 to that of Tyr-14, 3.46 ± 0.39 Å (range 2.63−4.38 Å), does not preclude hydrogen bonding between Asp-99 and Tyr-14.

A set of 11 intermolecular NOEs from isomerase to 19-NTHS which were incompatible with the productive mode of steroid binding (Figure 5B) were subsequently used separately to compute the structure of a nonproductive enzyme−steroid complex (Figure 9) which represents a second mode of 19-NTHS binding. The structural statistics from this nonproductive binding mode are given in Table 2. The nonproductive complex shows ∼90° rotation of the steroid about its long axis in accord with the affinity labeling of Asp-38 by diverse steroid epoxides (*29*, *30*).

Table 2: Structural Statistics of the Nonproductive Isomerase−19-NTHS Complex

Average RMSD from Idealized Geometry of 15 Structures			
bonds (Å)	$4.53 \times 10^{-3} \pm 5.35 \times 10^{-5}$		
angles (deg)	$6.94 \times 10^{-1} \pm 2.86 \times 10^{-2}$		
impropers (deg)	$1.159 \times 10^{\circ} \pm 4.71 \times 10^{-2}$		
Pairwise RMSD of an Ensemble of 15 Calculated Structures (Å)	**subunit 1**	**subunit 2**	**dimer**
backbone of secondary structure[a]	0.67 ± 0.10	0.73 ± 0.13	1.21 ± 0.38
all atoms, secondary structure	1.71 ± 0.15	1.79 ± 0.17	2.02 ± 0.25
all atoms, secondary KSI−NTHS	1.71 ± 0.15	1.79 ± 0.18	2.02 ± 0.24
backbone, residues 1−125	1.18 ± 0.30	1.10 ± 0.16	1.63 ± 0.44
all atoms, residues 1−125	2.09 ± 0.30	2.09 ± 0.18	2.42 ± 0.36
all atoms, KSI−NTHS	2.10 ± 0.30	2.08 ± 0.18	2.41 ± 0.36
all atoms, NTHS	1.12 ± 0.26	1.08 ± 0.24	1.63 ± 0.25

[a] Secondary structural elements for KSI−NTHS complex are residues 5−21, 23−30, 34−38, 44−47, 48−60, 63−67, 71−73, 78−87, 92−104, 111−116, and 121−124.

Quaternary Structure. The subunit interface of the enzyme was defined by 28 NOEs between hydrophobic residues in the ^{13}C-filtered NOESY−HSQC spectrum. As shown from the backbone superposition (Figure 6) and the pairwise RMSD values of the dimer (Table 1), the interface between the subunits is well-defined and is formed between the convex surfaces of the β-sheets. In addition to the hydrophobic residues, polar residues such as His-100, Arg-102, Arg-113, Arg-72, and Glu-77 are found in the interface (Figure 10). The His-100 side chain, which is buried in the interface, shows an exchangeable NϵH resonance at 12.8 ppm (*8*, *9*) which may participate in an intrasubunit hydrogen bond to Glu-77. The unusually low pK_a of 4.3 of His-100 (*8*, *13*) may be due to the electrostatic effects of the nearby cationic residues, Arg-102 and Arg-113. Residues at the interface do not interact with the substrate or form any cavity for ligand binding.

Comparison of the Structures of Free and Steroid-Bound Isomerase. The solution structure of the free enzyme from *Ps. testosteroni* was determined by Wu et al. (*6*). Super-

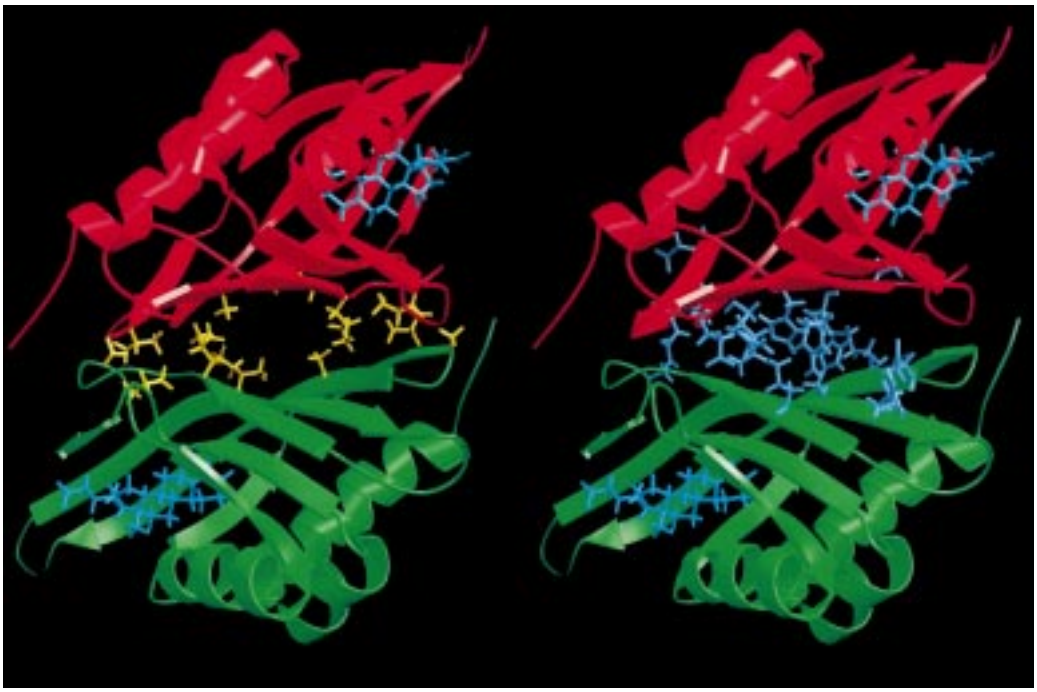

FIGURE 10: Lowest energy structure of the Δ^5-3-ketosteroid isomerase−19-NTHS complex showing hydrophobic (left) and polar residues (right) at the dimer interface. The bound steroid is in blue, as are the polar residues at the dimer interface. The hydrophobic residues are in yellow.

FIGURE 11: Superposition of the lowest energy solution structure of the Δ^5-3-ketosteroid isomerase complexed with 19-NTHS from this work (green) onto the solution structure of the free enzyme reported by Wu et al. (*6*) (red). For clarity the steroid has been omitted. Note the closer approach of the helices toward the β-sheet in the steroid-bound isomerase.

position of free and steroid-bound isomerase (Figure 11) reveals marked differences in the positions of the three α-helices which become more closely packed onto the concave surface of the β-sheet when substrate is bound, thereby allowing Tyr-14 to approach Asp-99 and the substrate more closely. The $^1H-^{15}N$ HSQC spectra of

Table 3: Comparison of the Solution Structure of Steroid-Bound Isomerase with the Solution Structure of Substrate-Free Isomerase (*6*)

	Pairwise RMSD of Liganded and Free Isomerase (Å)		
	subunit 1	subunit 2	dimer
productive steroid binding[a]			
backbone, secondary structure[b]	1.26 ± 0.11	1.30 ± 0.13	1.95 ± 0.59
backbone, α-helices	1.02 ± 0.11	1.03 ± 0.11	1.65 ± 0.47
backbone, β-sheet	1.25 ± 0.13	1.33 ± 0.17	1.94 ± 0.58
backbone, all residues	1.98 ± 0.19	1.99 ± 0.20	2.55 ± 0.57
nonproductive steroid binding[c]			
backbone, secondary structure	1.33 ± 0.15	1.38 ± 0.12	1.81 ± 0.33
backbone, α-helices	0.99 ± 0.09	1.00 ± 0.09	1.49 ± 0.29
backbone, β-sheet	1.39 ± 0.19	1.46 ± 0.17	1.85 ± 0.32
backbone, all residues	2.18 ± 0.30	2.16 ± 0.22	2.53 ± 0.40

[a] 15 NMR calculated structures consistent with the productive mode of substrate binding are superimposed. [b] Residues superimposed for the secondary structural elements are as follows: 5−21, 23−30, 34−38, 44−47, 48−60, 63−67, 71−73, 78−87, 92−104, 111−116, and 121−124. [c] 15 NMR calculated structures consistent with the nonproductive mode of substrate binding are superimposed.

isomerase in the free and steroid-bound states also reveal NH resonance shifts for residues surrounding the active site (*9*). Those residues that showed NH resonance shifts in the $^1H-^{15}N$ HSQC spectra show slightly different side-chain orientations in free and liganded isomerase, the most significant change being that of Tyr-14 which accepts a hydrogen bond from the side-chain carboxyl group of Asp-99 and donates a hydrogen bond to the 3-keto oxygen of the steroid. The distance between the Tyr-14-Oζ and Asp-99-COOHδ is 4.20 ± 0.67 Å in the free enzyme (*6*). We have previously shown that 19-NTHS binding to isomerase increases the order parameter of Tyr-14-CϵH for high-frequency motion, presumably due to hydrogen bonding of this residue in the complex (*32*). From the structure, other

Table 4: Comparison of NMR Solution Structures of Isomerase with the X-ray Structure of Free Isomerase from *Ps. putida* (*7*)

	Pairwise RMSD of NMR Structures with X-ray Structure (Å)		
	subunit 1	subunit 2	dimer
productive steroid binding vs crystalline free isomerase (*7*)[a]			
backbone, secondary structure[b]	1.27 ± 0.05	1.27 ± 0.07	2.81 ± 0.60
backbone, α-helices	1.17 ± 0.06	1.17 ± 0.08	2.47 ± 0.47
backbone, *β*-sheet	1.14 ± 0.06	1.14 ± 0.08	2.40 ± 0.55
nonproductive steroid binding vs crystalline free isomerase (*7*)[c]			
backbone, secondary structure	1.35 ± 0.05	1.34 ± 0.06	2.93 ± 0.47
backbone, α-helices	1.16 ± 0.04	1.15 ± 0.05	2.54 ± 0.34
backbone, *β*-sheet	1.30 ± 0.05	1.28 ± 0.09	2.56 ± 0.44
free isomerase in solution (*6*) vs crystalline free isomerase (*7*)[d]			
backbone, secondary structure	1.23 ± 0.12	1.19 ± 0.10	2.19 ± 0.29
backbone, α-helices	0.89 ± 0.09	0.88 ± 0.11	2.02 ± 0.27
backbone, *β*-sheet	1.24 ± 0.18	1.21 ± 0.14	1.85 ± 0.21

[a] 15 NMR calculated structures consistent with the productive mode of substrate binding are superimposed. [b] Residues superimposed for the secondary structural elements are as follows: NMR structures, 6−21, 24−30, 35−37, 44−47, 48−59, 63−67, 71−74, 78−86, 93−102, 111−115, and 121−123; X-ray structure, 8−23, 26−32, 37−39, 46−49, 50−61, 66−70, 74−77, 82−90, 97−106, 115−119, and 125−127. [c] 15 NMR calculated structures consistent with the nonproductive mode of substrate binding are superimposed. [d] 20 NMR calculated structures of substrate-free isomerase (*6*).

small changes in side-chain orientations at the active site occur upon steroid binding. Otherwise, the solution structures of free and steroid-bound isomerase are very similar. The pairwise superposition of the backbone Cα, C′, and N atoms of the secondary structural elements yielded pairwise RMSD values of 1.95 ± 0.59 Å for the dimer and 1.28 ± 0.12 Å for the individual subunits (Table 3). Superposition of the backbone Cα, C′, and N atoms of all residues yielded pairwise RMSD values of 2.55 ± 0.57 Å for the dimer and 1.99 ± 0.20 Å for the individual subunits.

Comparison of the solution structure of the isomerase−19-NTHS complex with the X-ray structure of the homologous unliganded isomerase from *Ps. putida* (*7*) was similarly performed. As found in the comparison with the solution structure of the free enzyme, steroid binding resulted in the movement of the helices toward the concave surface of the *β*-sheet, tightening down the active site. The pairwise superposition of the backbone atoms of the secondary structural elements of the liganded structures with the X-ray structure of the free enzyme yields pairwise RMSD values of 2.81 ± 0.60 Å for the dimer and 1.27 ± 0.06 Å for the individual subunits (Table 4). Although the X-ray structure of this isomerase complexed with dihydroequilenin, a reaction intermediate analogue, was also solved (at 2.5 Å resolution) as well as the free enzyme from *Ps. testosteroni* (at 2.3 Å resolution) (*12*), the coordinates are not available at the Brookhaven Protein Data Bank, and a comparison cannot therefore be performed. However, the X-ray structure of the steroid complex shows that the Asp-99 carboxyl and Tyr-14-OH are too far apart (3.87 Å) to form a hydrogen bond (*7*, *12*). Both Asp-99 and Tyr-14 donate hydrogen bonds to the 3-keto oxygen of the steroid. This result is inconsistent with the NMR-determined proximities of the Asp-99-COOH and Tyr-14-OH protons (*8*). Because ketosteroid isomerase can bind steroids in diverse orientations (*29*, *30*) (Figures 6 and 9) and because uncertainties in distances in a 2.5 Å X-ray structure can be as large as 0.75 Å (*24*), such differences in structure are possible.

Hydrogen bonding between Asp-99 and Tyr-14 has been criticized on the basis of the X-ray structure of isomerase from *Ps. testosteroni* which together with model building showed that the formation of such a hydrogen bond would result in the breakage of the hydrogen bond between Tyr-14 and Tyr-55 (*12*). However, since Asp-99 and Tyr-55 closely approach Tyr-14 from opposite directions in both the X-ray structure and our NMR structure, both hydrogen bonds can exist simultaneously. Moreover, the hydrogen bonding from Tyr-55 to Tyr-14 is unimportant to catalysis since the Y55F mutant shows only a 1.6-fold decrease in k_{cat}/K_m (*33*).

CONCLUSIONS

As found with the free enzyme (*6*), the solution structure of the isomerase−19-NTHS complex reveals the dimeric interface to be crowded with both polar and apolar residues. The active sites, which exist entirely on each individual subunit, consist of a hydrophobic groove between three α-helices and the concave surface of a mixed *β*-sheet. Comparison of the free and liganded enzyme indicates that substrate binding results in the movement of the helices toward the *β*-sheet, thereby tightening the active site and moving Tyr-14 closer to Asp-99 and to the 3-keto group of the substrate.

The solution structure of the enzyme−19-NTHS complex can accommodate the catalytic diad mechanism of isomerase action (Figure 1B) (*8*) in which the acid catalyst, Tyr-14, accepts a hydrogen bond from Asp-99 and donates a hydrogen bond to the 3-oxygen of the steroid. As the reaction proceeds to the dienolate intermediate, the hydrogen bond between Asp-99 and Tyr-14 becomes unusually strong, at least 7 kcal/mol (*4*, *8*). Presumably in the transition state, this hydrogen bond strengthening is transmitted to the Tyr−14−3-oxosteroid interaction, thereby facilitating carbonyl polarization and the concerted deprotonation of C4 by Asp-38. While the 2.5 Å X-ray structure of the dihydroequilenin complex of a homologous isomerase also indicates the Tyr-14−steroid interaction, it fails to detect the Asp-99···Tyr-14 interaction. Rather, direct hydrogen bonding of the 3-oxygen of the steroid by Asp-99 is seen, as in Figure 1A. This hydrogen bond is weaker or absent in solution. Hence, although less likely on the basis of the present solution structure, such a direct hydrogen bond, as in Figure 1A, cannot be excluded. As we have pointed out elsewhere (*24*), errors in individual distances as great as ±0.75 Å can occur in a 2.5 Å X-ray structure. Chemical shifts and fractionation factors of protons involved in hydrogen bonds (*8*, *24*), as incorporated into the present solution structure, can provide more precise determinations of hydrogen bond lengths with errors ≤0.05 Å.

ACKNOWLEDGMENT

We thank Dr. Paul Talalay for advice and encouragement throughout the course of this work.

SUPPORTING INFORMATION AVAILABLE

One table (Table S1) giving stereospecific proton and heteronuclear resonance assignments in the Δ^5-3-ketosteroid

isomerase−19-NTHS complex (8 pages). Ordering information is given on any current masthead page.

REFERENCES

1. Eames, T. C., Hawkinson, D. C., and Pollack, R. M. (1990) *J. Am. Chem. Soc.* 112, 1996−1998.
2. Holman, C. M., and Benisek, W. F. (1994) *Biochemistry 33*, 2672−2681.
3. Xue, L., Kuliopulos, A., Mildvan, A. S., and Talalay, P. (1991) *Biochemistry 30*, 4991−4997.
4. Zhao, Q., Abeygunawardana, C., Talalay, P., and Mildvan, A. S. (1996) *Proc. Natl. Acad. Sci. U.S.A. 93*, 8220−8224.
5. Kuliopulos, A., Talalay, P., and Mildvan, A. S. (1990) *Biochemistry 29*, 10271−10280.
6. Wu, R. W., Ebrahemian, S., Zawrotny, M. E., Thornberg, L. D., Perez-Alverado, G. C., Brothers, P., Pollack, R. M., and Summers, M. F. (1997) *Science 276*, 415−418.
7. Kim, S. W., Cha, S.-S., Cho, S.-S., Kim, J.-S., Ha, N.-C., Cho, M.-J., Joo, S., Kim, K. K., Choi, K. Y., and Oh, B.-H. (1997) *Biochemistry 36*, 14030−14036.
8. Zhao, Q., Abeygunawardana, C., Gittis, A. G., and Mildvan, A. S. (1997) *Biochemistry 36*, 14616−14626.
9. Zhao, Q., Abeygunawardana, C., and Mildvan, A. S. (1997) *Biochemistry 36*, 3458−3472.
10. Massiah, M. A., Gittis, A. G., Abeygunawardana, C., and Mildvan, A. S. (1998) *Abstracts, 39th Experimental NMR Conference*, March 22−27, Asilomar, CA, p 194, ENC, 1201 Don Diego Ave., Santa Fe, NM.
11. Massiah, M. A., Gittis, A. G., Abeygunawardana, C., and Mildvan, A. S. (1998) *Abstracts ASBMB Meeting*, May 17−20, Washington, DC; *FASEB J. 12*, A1360 (Abstract 290).
12. Cho, H.-S., Choi, G., Choi, K. Y., and Oh, B.-H. (1998) *Biochemistry 37*, 8325−8330.
13. Kuliopulos, A., Mullen, G. P., Xue, L., and Mildvan, A. S. (1991) *Biochemistry 30*, 3169−3178.
14. Wang, S.-F., Kawahara, F. S., and Talalay, P. (1963) *J. Biol. Chem. 258*, 576−585.
15. Ikura, M., and Bax, A. (1992) *J. Am. Chem. Soc. 114*, 2433.
16. Lee, W., Revington, M. J., Arrowsmith, C., and Kay, L. E. (1994) *FEBS Lett. 350*, 87.
17. Marion, D., Driscoll, P. C., Kay, L. E., Wingfield, P. T., Bax, A., Gronenborn, A. M., and Clore, C. M. (1989) *Biochemistry 28*, 6150−6156.
18. Jeener, J., Meier, B. H., Bachmann, P., and Ernst, R. R. (1979) *J. Chem. Phys. 71*, 4546−4553.
19. Macura, S., and Ernst, R. R. (1980) *Mol. Phys. 41*, 95−117.
20. Kuboniwa, H., Grzesiek, S., Delaglio, F., and Bax, A. (1994) *J. Biomol. NMR 4*, 871−878.
21. Zhu, G., and Bax, A. (1990) *J. Magn. Reson. 90*, 405−410.
22. Johnson, B. A., and Blevins, R. A. (1994) *J. Biomol. NMR 4*, 603.
23. McDermott, A., and Ridenour, C. F. (1996) in *Encyclopedia of NMR*, pp 3820−3824, J. Wiley & Sons Ltd., Sussex, England.
24. Mildvan, A. S., Harris, T. K., and Abeygunawardana, C. (1998) *Methods Enzymol.* (in press).
25. Kreevoy, M. M., and Liang, T. M. (1980) *J. Am. Chem. Soc. 102*, 3315−3322.
26. Precigoux, P. G., Busetto, B., Courseille, C., and Hospital, M. (1975) *Acta Crystallogr. B31*, 1527−1532.
27. Brünger, A. T. (1992) *X-PLOR (Version 3.1), A System for X-ray Crystallography and NMR*, Yale University Press, New Haven, CT.
28. Wüthrich, K. (1986) *NMR of Proteins and Nucleic Acids*, John Wiley & Sons, Inc., New York.
29. Bevins, C. L., Bantia, S., Pollack, R. M., Bounds, R. L., and Kayser, R. H. (1984) *J. Am. Chem. Soc. 106*, 4957−4962.
30. Bevins, C. L., Pollack, R. M., Kayser, R. H., and Bounds, P. L. (1986) *Biochemistry 25*, 5159−5164.
31. Xue, L., Talalay, P., and Mildvan, A. S. (1990) *Biochemistry 29*, 7491−7500.
32. Zhao, Q., Abeygunawardana, C., and Mildvan, A. S. (1996) *Biochemistry 35*, 1525−1532.
33. Kuliopulos, A., Mildvan, A. S., Shortle, D., and Talalay, P. (1989) *Biochemistry 28*, 149−159.
34. Kraulis, P. J. (1991) *J. Appl. Crystallogr. 24*, 946−950.
35. Merritt, E. A., and Bacon, D. J. (1997) *Methods Enzymol. 277*, 505−524.

BI981447B